Antiferroacoustic Resonances and Magnetoelastic Coupling in $GdAlO_3$

M. Boiteux, P. Doussineau, and B. Ferry
Laboratoire d'Ultrasons, Université Paris VI, Tour* 13,
11 *quai Saint-Bernard, Paris* 5e, *France*

and

U. T. Höchli
IBM Zurich Research Laboratory, 8803 *Rüschlikon, Switzerland*
(Received 17 February 1972)

Two resonances between spin waves and phonons are reported in the antiferromagnetic phase of $GdAlO_3$. The stronger of these resonances is the analog to the antiferromagnetic resonance observed by Rohrer and Blazey, and is consistent with free-energy parameters determining their phase diagram of $GdAlO_3$. The weaker line is attributed to a two-magnon, one-phonon process. These two resonances are observed with the magnetic field and the acoustic propagation vector along several symmetry axes. From their intensity the magnetoelastic coupling constants $|G_{11}| = 0.7$ cm^{-1} and $|G_{44}| = 0.3$ cm^{-1} are deduced. The diagonal elements of the elastic tensor and the corresponding sound velocities are also given.

I. INTRODUCTION

Antiferromagnetic $GdAlO_3$ has recently been the subject of a number of studies.[1-10] After its antiferromagnetic ordering had been found,[1] a complete phase diagram was established. Blazey and Rohrer[2] discovered that at zero field, antiferromagnetic ordering persists up to a Néel temperature $T_N = 3.9$ °K and, at zero temperature, up to a magnetic field of 11.5 kG, provided the field is in the direction of the easy axis. The critical field or spin-flop field is not observed if the misorientation angle is larger than 10°.[7,8]

The principal interest of this material lies in its weak exchange field of 19 kG which allows the investigation of different phases in a narrow and convenient temperature range and with easily accessible magnetic fields. Whereas the static properties of $GdAlO_3$ are now well investigated we shall here present experimental acoustic data which allow the determination of some of its dynamical properties.

The crystalline structure of $GdAlO_3$ is that of a perovskite with a slight orthorhombic distortion. Its space group is D_{2h}^{16} (*Pbmn*).[9] The elementary unit cell consists of four perovskite unit cells. Differential susceptibility[2,3] and magneto-optic-effect measurements of $GdAlO_3 : Er^{3+}$[4] have been performed and used to determine its magnetic structure. Below T_N it behaves as a uniaxial antiferromagnet consisting of two almost cubic sublattices. Each Gd^{3+} ion of the first sublattice has six nearest magnetic neighbors, also Gd^{3+} ions, of the second sublattice. The axis of easy magnetization coincides with the orthorhombic *b* axis as shown in Fig. 1.

This paper presents sound-velocity and attenuation data taken in the antiferromagnetic phase and at frequencies between 30 and 90 MHz, and at 9 GHz. From these data we shall deduce the strength of interaction between phonons and magnons and also confirm the presence of a soft-magnon mode driving the spin-flop transition. Such an investigation is normally conducted by neutron scattering, but in this case the large cross section of $GdAlO_3$ precludes the use of neutrons.[11] The use of high-frequency ultrasound allows one to separate the attenuation arising from resonance interaction with spin waves from the attenuation due to the spin-flop transition. This separation was not possible in similar experiments performed with relatively low-frequency sound.[12]

Ultrasonic-attenuation data covering a temperature range around T_N should also permit the determination of critical fluctuations of the magnetization. We shall present ultrasonic-attenuation data, but we are not in a position to deduce any critical

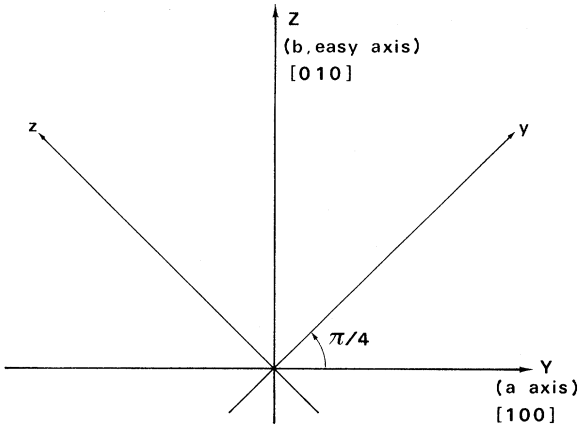

FIG. 1. Transformation of orthorhombic axes *y* and *z* into pseudocubic axes *y* and *z* in $GdAlO_3$.

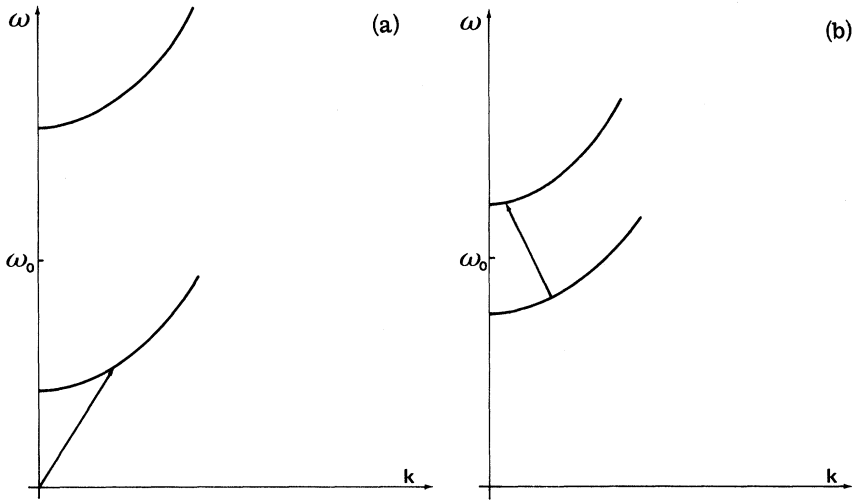

FIG. 2. Schematic presentation of (a) antiferromagnetic resonance process and (b) two-magnon transition.

parameter because of the relative weakness of the effect.

The remainder of this paper is divided into four sections. In Sec. II, the theory of magnetoelastic coupling is developed as a basis for the interpretation of the experimental data; the section starts from known excitations of both phonon and magnon type, and deduces values for the ultrasonic attenuation in terms of simple coupling constants. Section III is devoted to a description of the experimental apparatus and the experimental technique and then experimental results are presented: ultrasonic-attenuation data as a function of magnetic field up to 13 kG, temperature, and sound polarization and propagation. Sound-velocity data have also been taken at 30 MHz from below T_N to 400 °C; the high-temperature data represent an unsuccessful attempt to find a structural phase transition of $GdAlO_3$ by means of ultrasound. Comparison of experimental data with theoretical results allows the determination of magnetoelastic coupling constants of Gd^{3+} ion in $GdAlO_3$; Sec. IV contains a discussion of these findings. Finally, the results will be briefly summarized.

II. THEORY

We wish to establish a relation between the observed ultrasonic-absorption peaks and the spin-wave excitation spectrum of $GdAlO_3$. It is well known[13] that in an antiferromagnet there is one spin wave whose energy decreases monotonically with increasing applied magnetic field and tends to zero at some critical field H_c. The interaction of this mode with acoustic waves of a fixed frequency ω_{ac} gives rise to the acoustic-antiferromagnetic-resonance condition at a magnetic field given by $\omega_m = \omega_{ac}$.

A different process giving rise to ultrasonic attenuation is a transition between two antiferromagnetic spin waves. This process[6] is schematically drawn in Fig. 2. We shall calculate the ultrasonic attenuation due to either process for the case of $GdAlO_3$ by using a Hamiltonian which consists of a spin term, a strain term, and a coupling term. The excitations of the uncoupled systems, namely, the magnons in the antiferromagnetic phase, and the phonons, are used as basic functions for the coupling term, which will be evaluated using perturbation theory. We shall neglect fluctuations of the spin system due to the instability of the flop phase at the critical field, and treat the crystal as a homogeneous system. This is known as the molecular-field approximation which has proven useful in describing phase transitions of spin systems.

Thus our model Hamiltonian reads

$$\mathcal{H} = \mathcal{H}_P + \mathcal{H}_S + \mathcal{H}_{SP}, \tag{1}$$

where

$$\mathcal{H}_P = \tfrac{1}{2} C_{\alpha\beta} \epsilon_\alpha \epsilon_\beta + \tfrac{1}{2} \rho \left(\frac{\partial u}{\partial t}\right)^2, \tag{2}$$

$\epsilon = \partial u/\partial x$ denotes the strain, and u the displacement of the volume element at x. $\mathcal{H}_P$ has $k = 0$ acoustic phonons as eigenvalues. The spin part consists of three parts, namely,

$$\mathcal{H}_S = \mathcal{H}_E + \mathcal{H}_A + \mathcal{H}_Z, \tag{3}$$

where $\mathcal{H}_E$ is the exchange energy, $\mathcal{H}_A$ the anisotropy energy including the uniaxial crystalline anisotropy and the bilinear part of the anisotropic exchange, and $\mathcal{H}_Z$ the Zeeman energy. Expressed in spin variables these terms are given by

$$\mathcal{H}_E = \tfrac{1}{2} \sum_{ij} J_{ij} \vec{S}^i \cdot \vec{S}^j, \tag{4}$$

$$\mathcal{H}_A = \tfrac{1}{2} \sum_{ij} K_1 S_x^i S_x^j + K_2 \sum_{ij} [(S_x^i)^2 + (S_x^j)^2], \tag{5}$$

$$\mathcal{H}_Z = g\mu_B \sum_{ij} \vec{H}(\vec{S}^i + \vec{S}^j). \tag{6}$$

We first turn to the solutions of the spin part of the Hamiltonian which will give information as to spin-wave excitations. We shall then determine the spin-phonon coupling of those spin waves whose energies allow resonant interaction with sound at 9 GHz. The form of the coupling Hamiltonian $\mathcal{H}_{SP}$ will be derived in Sec. II B.

A. Magnons in the Long-Wavelength Limit

From the antiferromagnetic resonance (AFMR) frequency of 9.2 GHz and the sound velocity of the order of 5×10^5 cm/sec we conclude that both the magnon and the phonon involved in the resonance must have a wave vector $|k| \sim 10^5\,\mathrm{cm}^{-1}$. This is still small compared to the reciprocal-lattice distance. It seems therefore appropriate to consider the response of the average magnetic moment, rather than that of the individual spins, to perturbations and the molecular field. This procedure was initiated by Wangness[14] and carried out in detail by Thomas,[15] whom we follow. We solve

$$\frac{\partial\langle S\rangle}{\partial t} = -i\langle[S, \mathcal{H}_S]\rangle_t, \tag{7}$$

where $\mathcal{H}_S$ is given by Eq. (3). Evaluating the right-hand side with a density matrix in the molecular-field approximation and introducing relaxation times of the spin, Thomas postulates equations of motion for the ith spin in a molecular field $\vec{H}_i^{\,\mathrm{mol}}(t)$:

$$\frac{\partial\vec{\sigma}_i}{\partial t} = \vec{\sigma}_i \times \vec{H}_i^{\,\mathrm{mol}} - \frac{1}{\tau_1}(\vec{\sigma}_{i\parallel} - \vec{\sigma}_i) - \frac{1}{\tau_2}\vec{\sigma}_{i\perp}, \tag{8}$$

where $\vec{\sigma}_i = \langle\vec{S}_i\rangle/S$ and τ_1 and τ_2 account for relaxation of the spin components parallel and perpendicular to $\vec{H}_i^{\,\mathrm{mol}}$ towards equilibrium. The molecular field $\vec{H}_i^{\,\mathrm{mol}}$ and the average moment are related by

$$\sigma_i = B_S(g\mu_B \vec{H}_i^{\,\mathrm{mol}} \vec{S}/k_B T), \tag{9}$$

where

$$B_S(x) = \frac{2S+1}{2S}\coth\frac{(2S+1)x}{2S} - \frac{1}{2S}\coth\frac{x}{2S} \tag{10}$$

is the Brillouin function. From this he obtains the response of σ_i to a periodic external field defined as dynamic susceptibility $\chi_{ij}(\omega)$ by

$$\delta\sigma_i = \sum_j \chi_{ij}(\omega)\,\delta H_j. \tag{11}$$

The result is

$$\chi_{ij}^{-1}(\omega) = \chi_{ij}^{-1} - i\left(\frac{\tau_1}{\chi_{i\parallel}} P_{i\parallel} + \frac{\tau_2}{\chi_{i\perp}} \times (1 - \vec{H}_i^{\,\mathrm{mol}}\tau_2\epsilon_{i\perp})^{-1} P_{i\perp}\right)\delta_{ij}. \tag{12}$$

Here

$$\chi_{ij}^{-1} = \frac{\partial^2 F}{\partial\langle S_i\rangle\,\partial\langle S_j\rangle} \tag{13}$$

is the static reciprocal susceptibility,

$$k_\parallel = \frac{k_B T}{S^2}\frac{\partial B^{-1}(\sigma)}{\partial\sigma}, \tag{14}$$

$$\chi_\perp = \frac{k_B T}{S^2}\frac{B^{-1}(\sigma)}{\sigma}, \tag{15}$$

and $\vec{P}$ is a unit polarization vector in the direction of $\vec{H}_i^{\,\mathrm{mol}}$; ϵ is the antisymmetric unit tensor of rank 2 and F the free energy of the spin system.

The spatial Fourier transform of Eq. (12) leads to

$$\chi_q^{-1}(\omega) = \chi_q^{-1} - i\omega\left(\frac{\tau_1}{\chi_\parallel} P_\parallel + \frac{\tau_2}{\chi_\perp}(1 - H^{\mathrm{mol}}\tau_2\epsilon_\perp)^{-1} P_\perp\right). \tag{16}$$

The secular equation determining the eigenfrequencies can be written

$$\det\left(\frac{\chi_\parallel}{\tau_1} P_\parallel + \frac{\chi_\perp}{\tau_2}(1 - H^{\mathrm{mol}}\tau_2\epsilon_\perp)P_\perp \chi_q^{-1} - i\Omega_q I\right) = 0. \tag{17}$$

We solved Eq. (17) by a computer in the following sequence: First, the equilibrium configuration was computed using the condition $F(\sigma) = \min$. In an antiferromagnet, $\vec{\sigma}$ has six components, three for each sublattice. The static susceptibility was taken from the free energy including demagnetization which is given by

$$\begin{aligned} F/S^2 = {} & J_1'\,\sigma_A\sigma_B[\cos(\alpha-\beta)\sin\varphi\sin\theta + \cos\varphi\cos\theta] + \tfrac{1}{2}J_2'(\sigma_A^2+\sigma_B^2) + K_1'\sigma_A\sigma_B\cos\alpha\cos\beta\sin\varphi\sin\theta \\ & + \Delta K_1'\sigma_A\sigma_B\cos\varphi\cos\theta + \tfrac{1}{2}K_2'(\sigma_A^2\cos^2\alpha\sin^2\varphi + \sigma_B^2\cos^2\beta\sin^2\theta) + \tfrac{1}{2}\Delta K_2'(\sigma_A^2\cos^2\varphi + \sigma_B^2\cos^2\theta) - (g\mu_B/S) \\ & \times H_{\mathrm{ext}}\{\sigma_A[\cos(\alpha-\psi)\sin\varphi\sin\rho + \cos\varphi\cos\rho] + \sigma_B[\cos(\beta-\psi)\sin\theta\sin\rho + \cos\theta\cos\rho]\} - (T/S^2)[b(\sigma_A) + b(\sigma_B)] \\ & + N_{xy}[\sigma_A^2\sin\alpha\sin\varphi\cos\varphi + \sigma_B^2\sin\beta\sin\theta\cos\theta + \sigma_A\sigma_B(\sin\alpha\sin\varphi\cos\theta + \sin\beta\cos\varphi\sin\theta)] \\ & + N_{xz}[\sigma_A^2\sin\alpha\cos\alpha\sin^2\varphi + \sigma_B^2\sin\beta\cos\beta\sin^2\theta + \sigma_A\sigma_B(\sin\alpha\cos\beta + \cos\alpha\sin\beta)\sin\varphi\sin\theta] \\ & + N_{yz}[\sigma_A^2\cos\alpha\sin\varphi\cos\varphi + \sigma_B^2\cos\beta\sin\theta\cos\theta + \sigma_A\sigma_B(\cos\alpha\sin\varphi\cos\theta + \cos\beta\cos\varphi\sin\theta)], \end{aligned} \tag{18}$$

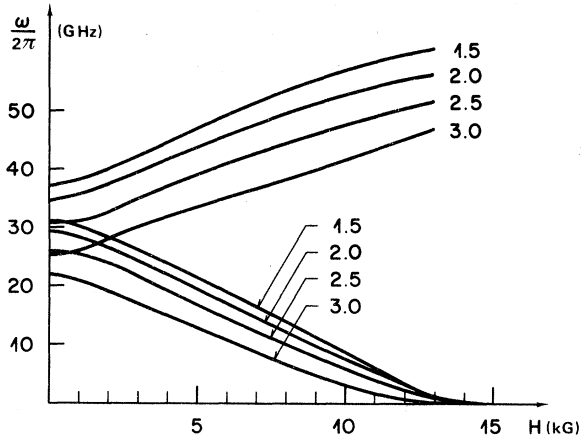

FIG. 3. Theoretical spin-wave spectrum in the flop phase (based on parameters determined in Ref. 16).

where

$$J_1' = J_1 + N_{xx}\ , \qquad J_2' = J_2 + N_{xx}\ ,$$

$$K_1' = K_1 + (N_{zz} - N_{xx})\ , \quad \Delta K_1' = \Delta K_1 + (N_{yy} - N_{xx})\ , \tag{19}$$

$$K_2' = K_2 + (N_{zz} - N_{xx})\ , \quad \Delta K_2' = \Delta K_2 + (N_{yy} - N_{xx})\ .$$

Here σ_A, α, and φ are polar coordinates for the average value $\vec{\sigma}_A$ of the spins of sublattice A. Similarly σ_B, β, and θ are polar coordinates for $\vec{\sigma}_B$, and the magnetic field is expressed in coordinates H, ψ, ρ. J_1, K_1, and ΔK_1 are the intersublattice, J_2, K_2, and ΔK_2 the intrasublattice coupling constants. J accounts for isotropic coupling, K for axial anisotropy along the easy direction, and ΔK for anisotropy of the coupling along the y direction. T is the temperature and $b(\sigma_A)$ and $b(\sigma_B)$ are the entropies per spin of sublattices A and B.

The terms in N_{jk} are demagnetizing factors, depending on the orientation and shape of the sample. They are obtained by a transformation of the demagnetizing tensor for a plate in its own coordinate system

$$N = \begin{pmatrix} 0 & & \\ & 0 & \\ & & 4\pi \end{pmatrix} \tag{20}$$

into the coordinate system of the crystalline anisotropy.

Next, the dynamic susceptibility was computed by means of Eq. (17). The relaxation times used were those determined by Thomas and Rohrer.[16] Finally, the solution of the secular equation gave values for the eigenfrequencies in the antiferromagnetic (AF) state. They are plotted in Fig. 3 for the case of a $GdAlO_3$ sample cut along the directions [001], [110], and [1$\bar{1}$0] in an external magnetic field applied along the [010] direction. Removal of the degeneracy of the spin-wave modes in zero field is due to the effect of the sample form.[17] It is seen that there is a soft-magnon branch with a temperature-dependent thermodynamic critical field around 13 kG. The soft-magnon branch is expected to interact resonantly with 9-GHz acoustic waves at all temperatures in the AF state, whereas the hard-magnon branch has too high an energy to do that.

The field at which $\omega_m = \omega_{ac}$ is plotted versus temperature in Fig. 4. This has to be compared with the experimental attenuation maximum also plotted in the same figure. There is good agreement between the observed and the computed line positions. Note that the computation rests on the molecular-field approximation which gives a slight discrepancy for the magnitude of the spin-flop field, also shown in Fig. 4.

B. Magnon-Phonon Coupling

Time-reversal symmetry precludes coupling between spin and strain which is linear in spin variables. Instead there are two major indirect coupling mechanisms which we shall consider in turn in order to construct the coupling Hamiltonian.

1. Volume Magnetostriction

The dependence of interaction between spins S_i and S_j on their distance r_{ij} gives rise to an effective coupling of the form[18]

$$\mathcal{H}_{\text{vol}} = \sum_{i \neq j} \vec{\nabla}(r_{ij})\, K(r_{ij}) \vec{\delta} r_{ij} f(\vec{S}^i, \vec{S}^j), \tag{21}$$

where $\vec{\nabla}$ is the gradient vector, K the interaction constant, and $f(\vec{S}^i, \vec{S}^j)$ a bilinear function of S. Mechanisms which contribute to volume magnetostriction are the exchange modulation,[19] magnetic

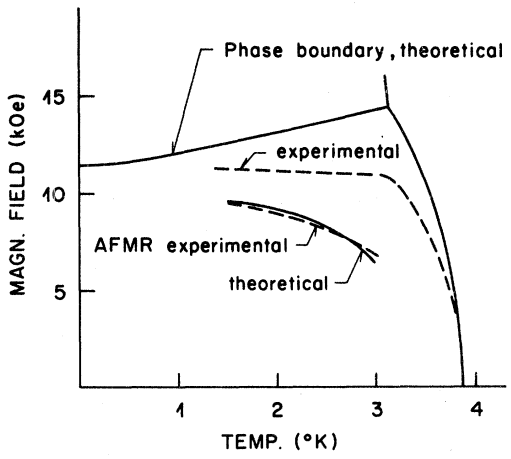

FIG. 4. Phase diagram and resonance condition for acoustic AFMR in $GdAlO_3$, theoretical and experimental. Phase diagram after Ref. 7.

dipolar interaction,[20] and coupling to the phonon field.[21] An order-of-magnitude estimate shows that exchange modulation gives by far the largest contribution to the effective magnetostriction. It is of the form

$$f(\vec{S}^i, \vec{S}^j) = \vec{S}^i \cdot \vec{S}^j = \tfrac{1}{2}(S_+^i S_-^j + S_-^i S_+^j) + S_z^i S_z^j . \quad (22)$$

2. Single-Ion Magnetostriction

This mechanism, introduced by Van Vleck,[22] consists in an effective spin-phonon coupling provided by spin-orbit interaction and orbit-lattice interaction. To first order in the strain

$$\mathcal{H}_{SI} = \sum_l \sum_{\alpha\beta\gamma\delta} G_{\alpha\beta\gamma\delta} S_\alpha^l S_\beta^l \epsilon_{\gamma\delta} . \quad (23)$$

G is the magnetoelastic coupling tensor whose relations between components are determined by the symmetry of the site. The summation index l extends over the spins of the whole crystal. Finite deformation terms are omitted throughout this paper, in accordance with Eastman[23] but in contrast to Melcher[24] who finds them necessary to account for his data in MnF_2. The terms of the interaction Hamiltonian which give rise to acoustic antiferromagnetic resonance with $\Delta M = 1$ are linear in both strain and spin operators S_+ or S_-. Those terms which give rise to transitions between two spin waves, i.e., $\Delta M = 2$ processes, are quadratic in the spin operators S_+ or S_- and linear in the strain operators. These selection rules preclude terms due to exchange modulation,[25] while single-ion magnetostriction contribute to both $\Delta M = 1$ and $\Delta M = 2$ processes.

The interaction Hamiltonian thus depends only on single-ion magnetostriction for ions on both sites,

$$\mathcal{H}_{int} = \mathcal{H}_{SI}^i + \mathcal{H}_{SI}^j . \quad (24)$$

We shall ignore the departure of $GdAlO_3$ from cubic symmetry and obtain two identical terms for each sublattice of the form

$$\mathcal{H}_{int}^i = \sum_{i=1}^N \{ \tfrac{1}{2} G_{11} [(3S_x^{i2} - S^2)\epsilon_{xx} + (3S_y^{i2} - S^2)\epsilon_{yy} + (3S_z^{i2} - S^2)\epsilon_{zz}] + 2G_{44} [\{S_x^i, S_y^i\}\epsilon_{xy} + \{S_y^i, S_z^i\}\epsilon_{yz} + \{S_x^i, S_z^i\}\epsilon_{xz}] \} , \quad (25)$$

where

$$\{S_\alpha, S_\beta\} = S_\alpha S_\beta + S_\beta S_\alpha .$$

We shall express this coupling Hamiltonian in terms of creation and annihilation operators of phonons and magnons. First the spin components are transformed into orthorhombic coordinates X, Y, and Z, where [010] denotes the easy axis and is at the same time the spin quantization axis Z (see Fig. 1) with

$$\begin{pmatrix} S_x \\ S_y \\ S_z \end{pmatrix} = \begin{pmatrix} 1 & 0 & 0 \\ 0 & 1/\sqrt{2} & 1/\sqrt{2} \\ 0 & -1/\sqrt{2} & 1/\sqrt{2} \end{pmatrix} \begin{pmatrix} S_X \\ S_Y \\ S_Z \end{pmatrix} . \quad (26)$$

One finds

$$\mathcal{H}_{int} = \sum_{i=1}^N \left(\tfrac{3}{2} G_{11} (S_X^{i2} - S^2)\epsilon_{xx} + \tfrac{1}{2} G_{11} [\tfrac{3}{2} (S_Z^{i2} + S_Y^{i2} + \{S_Z^i, S_Y^i\} - S^2)] \epsilon_{yy} + \tfrac{1}{2} G_{11} [\tfrac{3}{2} (S_Z^{i2} + S_Y^{i2} - \{S_Z^i, S_Y^i\}) - S^2] \epsilon_{zz} + G_{44}\sqrt{2} (\{S_X^i, S_Z^i\} + \{S_X^i, S_Y^i\})\epsilon_{xy} + G_{44}\sqrt{2} (\{S_X^i, S_Z^i\} - \{S_X^i, S_Y^i\})\epsilon_{xz} + 2 G_{44} (S_Z^{i2} - S_Y^{i2})\epsilon_{yz} \right) , \quad (27)$$

plus a similar term for the second sublattice.

An inspection of this Hamiltonian shows that $\Delta M = 1$ transitions are induced by strains ϵ_{yy}, ϵ_{zz}, ϵ_{xy}, and ϵ_{xz}, whereas $\Delta M = 2$ transitions are induced by all strains. The ultrasonic-attenuation coefficients can be evaluated by use of the Golden rule,

$$\alpha = \frac{1}{v} \frac{2\pi}{\hbar^2} |\langle i | \mathcal{H}_{int} | f \rangle|^2 \delta(\omega) , \quad (28)$$

with i and f denoting initial and final states, respectively, and v the sound velocity. Evaluation of Eq. (28) will be performed only for particular propagation directions for which experimental data are available.

C. Ultrasonic-Attenuation Coefficients

1. Antiferromagnetic Acoustic Resonance

For longitudinal waves in the y direction ([110] axis) the only nonvanishing strain is ϵ_{yy}, and Eq. (27) reduces to

$$\mathcal{H}_{int} = \tfrac{1}{2} G_{11} \sum_{i=1}^N [\tfrac{3}{2} (S_Z^{i2} + S_Y^{i2} + \{S_Z^i, S_Y^i\}) - S^2] \epsilon_{yy} + \tfrac{1}{2} G_{11} \sum_{j=1}^N [\tfrac{3}{2} (S_Z^{j2} + S_Y^{j2} + \{S_Z^j, S_Y^j\}) - S^2] \epsilon_{yy} . \quad (29)$$

Keeping only terms giving rise to a resonant process between one phonon and one magnon,

$$\mathcal{H}_{\rm int}=\tfrac{3}{4}G_{11}\Big(\sum_{i=1}^{N}\{S_Z^i,S_Y^i\}+\sum_{j=1}^{N}\{S_Z^j,S_Y^j\}\Big)\epsilon_{yy} \tag{30}$$

is obtained.

Expressed in magnon operators a and b defined by the Holstein-Primakoff transformation of spin operators followed by a Fourier transform,[13] the interaction Hamiltonian reads

$$\mathcal{H}_{\rm int}=\tfrac{3}{4}G_{11}S(2S)^{1/2}[(a_q-a_{-q}^{\dagger}+b_{-q}-b_q^{\dagger})c_q - (a_{-q}-a_q^{\dagger}+b_q-b_{-q}^{\dagger})c_q^{\dagger}] , \tag{31}$$

where $c_q^{\dagger}$ and c_q are creation and annihilation operators of phonons defined in the following manner:

$$\epsilon_{yy}=(\hbar\omega_q/2\rho v_{yy}^2V)^{1/2}i(c_qe^{i\vec{q}\cdot\vec{R}_i}-c_q^{\dagger}e^{-i\vec{q}\cdot\vec{R}_i}) . \tag{32}$$

Here $\omega_q/2\pi$ is the frequency of applied ultrasonic waves, v_{yy} is the velocity of sound propagating in the y direction and polarized along y, and ρV is the mass of crystal. The spin waves have been assumed to be noninteracting.

In order to obtain a representation which diagonalizes the energy of the spin system, we apply the Bogoliubov transformation to the magnon operators,

$$\begin{aligned} a_k&=\alpha_k\cosh\theta_k+\beta_k^{\dagger}\sinh\theta_k ,\\ b_k&=\alpha_k^{\dagger}\sinh\theta_k+\beta_k\cosh\theta_k , \end{aligned} \tag{33}$$

with

$$\tanh2\theta_k=-H_E\gamma_k/(H_E+H_A) ,$$

where γ_k is defined in the usual way:

$$\gamma_k=(1/z)\textstyle\sum_{\delta}e^{i\vec{k}\cdot\vec{\delta}} .$$

H_E is the exchange field, H_A the anisotropy field, and z the number of nearest neighbors. The result of the transformation is

$$\begin{aligned}\mathcal{H}_{\rm int}=&\tfrac{3}{4}G_{11}S(2S)^{1/2}(\hbar\omega_q/4\rho v^2)^{1/2}(\cosh\theta_q-\sinh\theta_q)\\ &\times\{[(\alpha_q-\alpha_{-q}^{\dagger})+(\beta_{-q}-\beta_q^{\dagger})]c_q\\ &-[(\alpha_{-q}-\alpha_q^{\dagger})+(\beta_q-\beta_{-q}^{\dagger})]c_q^{\dagger}\} .\end{aligned} \tag{34}$$

Only terms corresponding to the low-frequency branch of spin modes need to be retained; thus

$$\begin{aligned}\mathcal{H}_{\rm int}=&\tfrac{3}{4}G_{11}S(2S)^{1/2}(\hbar\omega_q/4\rho v^2a^3)^{1/2},\\ &\times(\cosh\theta_q-\sinh\theta_q)(c_q\beta_q^{\dagger}+c_q^{\dagger}\beta_q) ,\end{aligned} \tag{35}$$

where a is the parameter of the pseudocubic unit cell. Since we are interested in the ultrasonic attenuation as a function of the magnetic field around H_c it is practical to introduce a spin-wave linewidth g arising from a lifetime T_2,

$$g(\omega-\omega_\beta)=(T_2/\pi)[1+T_2^2(\omega-\omega_\beta)^2]^{-1} . \tag{36}$$

Straightforward algebra shows that maximum attenuation occurs at ω_β and is given by

$$\alpha\,\mathrm{dB/cm}=0.6G_{11}^2S^3(\omega_q/\rho v^3a^3\hbar)(\cosh\theta_q-\sinh\theta_q)^2T_2 . \tag{37}$$

Experimental determination of the absorption maximum and the relaxation time T_2 from the resonance linewidth allows in this case the coupling constant G_{11} to be evaluated.

Leaving the magnetic field in the direction of the easy axis but changing the polarization and propagation vector of the sound we obtain other effective coupling constants. In particular for $\vec{q}\parallel[001]$ and $\vec{u}\parallel[010]$, where $\vec{q}$ denotes the wave vector and $\vec{u}$ the direction of the displacement, the only nonvanishing strains are ϵ_{xy} and ϵ_{xz}. The ultrasonic attenuation is then given by

$$\alpha=2.15\,|G_{44}|^2(S^3\omega_q/\rho v^3a^3\hbar)(\cosh\theta_q+\sinh\theta_q)^2T_2 . \tag{38}$$

2. *Transition between Two Spin-Wave Modes*

Longitudinal waves in the [010] direction imply $\epsilon_{yy}=\epsilon_{zz}=\epsilon_{yz}\neq0$. Keeping only two-magnon and one-phonon operators in Eq. (27) one obtains

$$\begin{aligned}\mathcal{H}_{\rm int}=&\,i(\hbar/2\rho v^2V)^{1/2}\textstyle\sum_k\{(\frac{3}{2}G_{11}-2G_{44})\\ &\times[c_q(a_ka_{-k+q}+a_k^{\dagger}a_{-k-q}^{\dagger}+b_k^{\dagger}b_{-k+q}^{\dagger}+b_kb_{-k-q})\\ &-c_q^{\dagger}(a_ka_{-k-q}+a_k^{\dagger}a_{-k+q}^{\dagger}+b_kb_{-k+q}+b_k^{\dagger}b_{-k-q}^{\dagger})]\\ &-2(3G_{11}+4G_{44})[c_q(a_k^{\dagger}a_{k+q}+b_k^{\dagger}b_{k-q})\\ &-c_q^{\dagger}(a_k^{\dagger}a_{k-q}+b_k^{\dagger}b_{k-q})]\} .\end{aligned} \tag{39}$$

Assuming the phonon energy is less than twice the magnon energies one can simplify by excluding double creation or annihilation. In this case, application of the Bogoliubov transform on operators a and b yields

$$\begin{aligned}\mathcal{H}_{\rm int}=&\,2i(\hbar\omega_1/2\rho v^2V)^{1/2}(\tfrac{3}{2}G_{11}-2G_{44})\\ &\times\textstyle\sum_k\sinh(\theta_k+\theta_{-k-q})[\alpha_k^{\dagger}\beta_{-k-q}c_q-\alpha_k\beta_{-k-q}^{\dagger}c_q^{\dagger}] .\end{aligned} \tag{40}$$

Here, we also take into account the linewidth due to the finite magnon lifetime. The attenuation then becomes

$$\begin{aligned}\alpha=&\frac{\pi}{\hbar^2}\frac{S^2(\frac{3}{2}G_{11}-2G_{44})^2}{\rho v^3}\hbar\omega_q\\ &\times\sum_k\sinh^2(\theta_k+\theta_{-k-q})(n_{-k-q}^{\beta}-n_k^{\alpha})g(\omega_\alpha-\omega_\beta-\omega_q) .\end{aligned} \tag{41}$$

The sum over k can be replaced by an integral over the Brillouin zone,

$$\sum_k\rightarrow\frac{V}{(2\pi)^2}\iint k^2\sin\theta\,d\theta\,dk . \tag{42}$$

We put $\gamma_k=\frac{1}{3}(1+2\cos\frac{1}{3}ka)$ and obtain

$$\alpha = \frac{4.3}{16\pi^2} S^2 \frac{\omega_q^2 (\frac{3}{2} G_{11} - 2G_{44})^2}{\rho v^3 a^3} T_2 \frac{1}{k_B T} I , \qquad (43)$$

where

$$I = \int_0^\pi a^2 k^2 d(ak) \sinh^2(\theta_k + \theta_{-k-q}) \frac{e^{\hbar \omega_k / k_B T}}{(e^{\hbar \omega_k / k_B T} - 1)^2} . \qquad (44)$$

The integral in Eq. (44) accounts for the contributions of all spin waves with frequency $\omega(k)$.

For other ultrasonic polarization and propagation directions, a similar expression for the attenuation is obtained; only the coupling constant G changes. In particular, for longitudinal waves $\vec{q} \parallel \vec{u} \parallel [001]$ the attenuation is given by

$$\alpha = 4.3 \frac{9}{32\pi^2} G_{11}^2 S^2 \frac{\omega_q^2}{\rho v^3 a^3 k_B T} T_2 I , \qquad (45)$$

with I as before.

III. EXPERIMENTS

A. Experimental Technique

By means of a method by Jacobsen[26] 9-GHz ultrasonic waves are generated. For reflection measurements a quartz transducer is glued on a $GdAlO_3$ sample and mounted in a reentrant cavity such that the quartz surface is mechanically excited by the piezoelectric effect. The electric field is generated by a tunable magnetron with an output of 10 kW at 8.5–9.5 GHz. The reflected ultrasonic wave is detected by means of a classical heterodyne receiver making use of the inverse piezoelectric effect. For transmission measurements a system of two identical cavities is used where the sample is attached to two quartz transducers.

The ultrasonic attenuation was measured as a function of temperature and magnetic field. The signal received is fed into a boxcar integrator to enhance the signal-to-noise ratio, and can be recorded as a function of some varying parameter.

Figure 5 shows such a record: The ultrasonic attenuation is given as a function of the magnetic field for a fixed temperature of 1.7 °K. Temperature control was achieved by regulating the pressure above the liquid-helium bath. Allen-Bradley carbon resistors were used to measure the temperature.

$GdAlO_3$ samples were grown from a PbO-PbF_2-B_2O_3 solution[27] and oriented by x rays to better than $\frac{1}{2}°$. Most data were taken on different thin plates with thicknesses of 0.15–1 mm along the [001], [010], and [110] directions. The surfaces were optically polished to allow a plane wave to propagate through the surfaces. In all measurements the external magnetic field was applied in

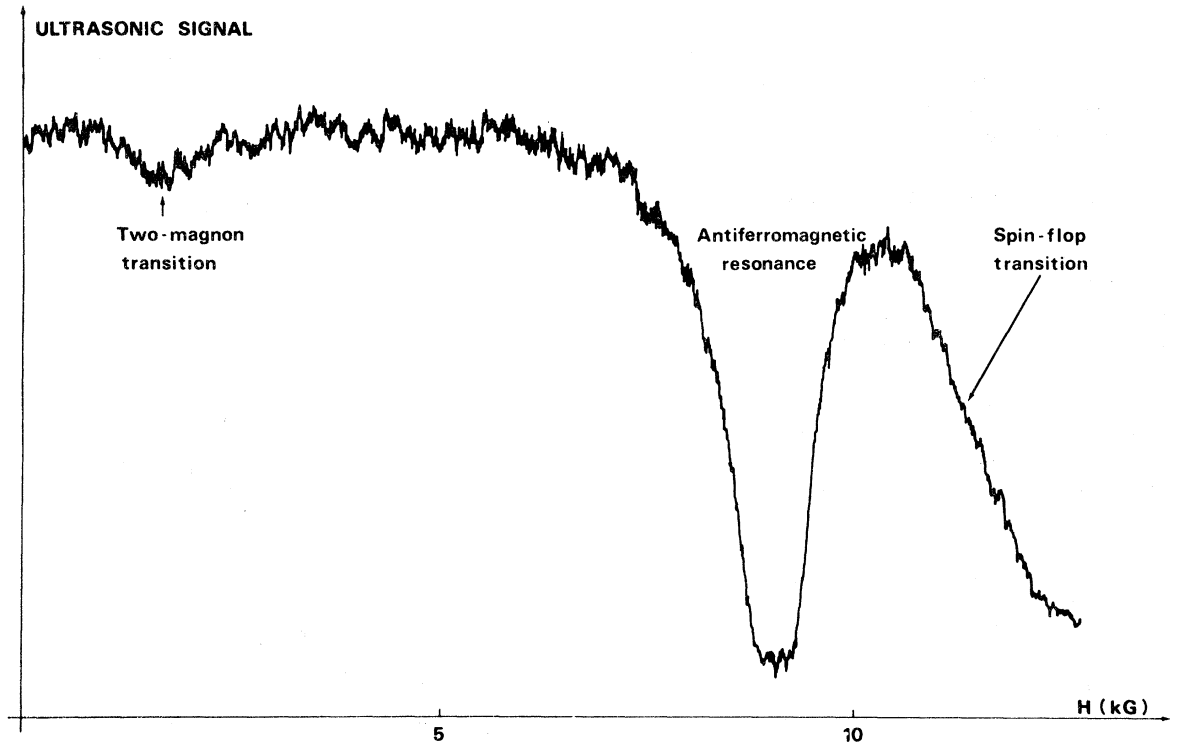

FIG. 5. Ultrasonic signal as a function of magnetic field applied in the [010] direction of $GdAlO_3$. Ultrasonic waves have $f = 8.6$ GHz, are polarized along [001], and propagate along [110]. $T = 1.7$ °K.

TABLE I. Experimental data. All data have been taken at an ultrasonic frequency of 9 GHz and at a temperature of 1.7°K. Only exception: fifth line, $\vec{k} \parallel [001]$, $\vec{u} \parallel [010]$, temperature = 2.65°K.

	Sound velocity (10^5 cm/sec)	Low-field line	Resonance line	Attenuation in flop phase (dB/cm)
$\vec{k} \parallel [010]$, $\vec{u} \parallel [010]$	7.3 ± 0.3	(1650 ± 100) G 1 dB/cm		>100
$\vec{k} \parallel [001]$, $\vec{u} \parallel [001]$	6.6 ± 0.3	(1750 ± 100) G 0.5 dB/cm		~15
$\vec{k} \parallel [110]$, $\vec{u} \parallel [110]$	6.3 ± 0.3		9100 G 1200 dB/cm	~50
$\vec{k} \parallel [110]$, $\vec{u} \parallel [001]$	4.0 ± 0.3	(1650 ± 100) G 0.7 dB/cm	9100 G 100 dB/cm	~ 5
$\vec{k} \parallel [001]$, $\vec{u} \parallel [010]$	4.3 ± 0.3		7700 G 14 dB/cm	~10
$\vec{k}$ [110], $\vec{u}$ [1$\bar{1}$0]	4.8 ± 0.3			>20

the b direction. Alignment of the sample with respect to the external field was checked by means of the position of the AFMR line which occurs in a magnetic field minimum if the misalignment angle is null.

B. Experimental Results

Attenuation data have been taken for the following ultrasonic polarizations; the corresponding sound velocities are given in Table I.

a. Longitudinal waves with $\vec{k} \parallel \vec{u} \parallel b$. An ultrasonic-absorption line of 0.7-dB/cm amplitude is observed at an applied field of (1650 ± 100) G. It has a linewidth of 1000 G at 1.6 °K and broadens rapidly beyond detection at 2.2 °K (Fig. 6). Its position, however, is temperature independent. No absorption line is observed at 9 kG unless the magnetic field is misaligned by at least 0.5°. Above 12 kG the ultrasonic absorption becomes very large, $\alpha > 50$ dB/cm.

b. $\vec{k} \parallel \vec{u} \parallel c$. The same behavior is found for the 1650-G line and for the 12-kG absorption edge as in the previous case.

c. $\vec{k} \parallel \vec{u}$ [110], *at* 45° *to b*. No absorption line is detected at 1650 G but the 9-kG line is very strong (1200 dB/cm). Its position and its linewidth were measured as a function of temperature (Figs. 6 and 7) between 1.6 and 3.5 °K. The 12-kG absorption edge is again observed, but it is less strong than for the preceding configurations.

d. Transverse waves, $\vec{k} \parallel [110] \vec{u} \parallel [001]$. All three lines are observed (Fig. 5).

e. $\vec{k} \parallel [001] \vec{u} \parallel [010]$. Attenuation is observed only in the flop phase.

f. $\vec{k} \parallel [001] \vec{u} \parallel [010]$. Same as 3.

Ultrasonic absorption was also measured as a function of temperature at zero magnetic field. Only two cases yield any information.

(i) For $\vec{k} \parallel \vec{u} \parallel [110]$ an attenuation maximum is found at 3.5 °K, just slightly below the Néel temperature. The line is 0.3° wide and has an ampli-

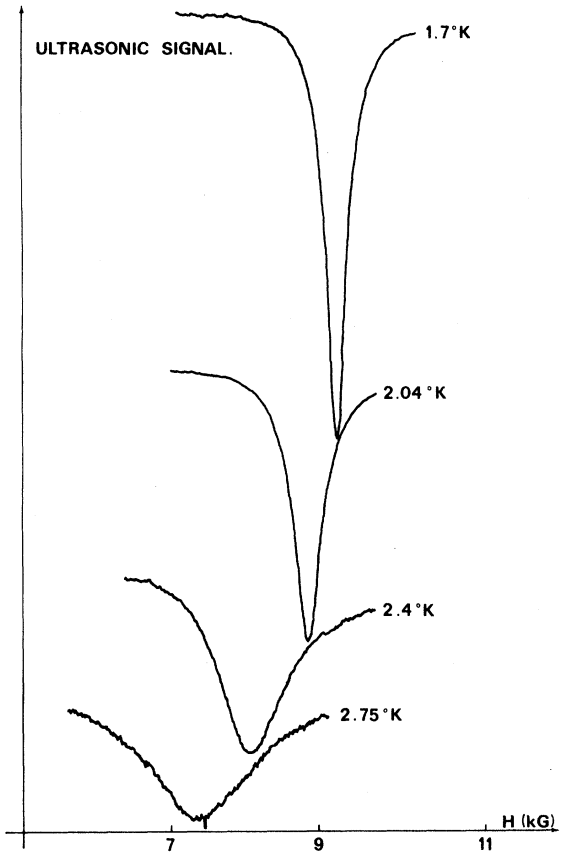

FIG. 6. Acoustic antiferromagnetic resonance in $GdAlO_3$. Magnetic field along [010]. Ultrasonic polarization and propagation along [110]. $f = 9$ GHz (the shift of the curves along the vertical axis is quite arbitrary).

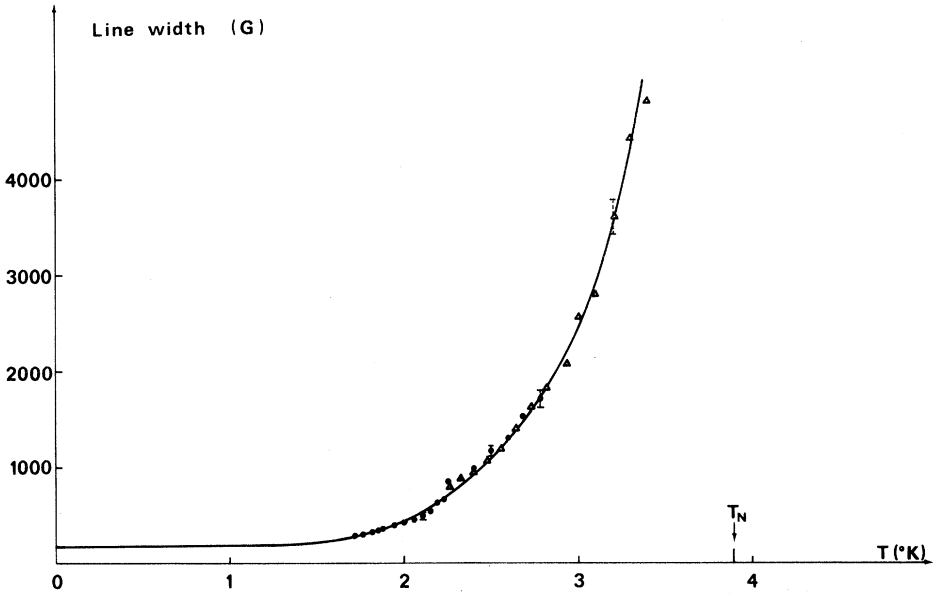

FIG. 7. Width of antiferromagnetic acoustic resonance in $GdAlO_3$ as a function of temperature. Circles: data points from sample with 0.15-mm thickness; triangles: same with 1-mm thickness.

tude of 1 dB/cm.

(ii) For $\vec{k} \parallel [110]\, \vec{u} \parallel [001]$ the attenuation maximum is observed at the Néel temperature. Its amplitude is 4 dB/cm, the width about 1°. The data are shown in Fig. 8 and summarized in Table I. Separate values for the coupling constants G_{11} and G_{44} were deduced from each measurement of the absorption amplitude. Sound-velocity data were also taken at 30 and 90 MHz using pulse-superposition techniques. To the experimental accuracy of 10^{-5} for relative measurements there was no sign of any phase change from 1.4 to 400 °K but, a slight softening of elastic constants at elevated temperature. The sound velocities at room temperature are given in meters per second:

$$V_{xx} = 6250 \pm 2\,, \quad V_{xy} = 3690 \pm 10\,, \quad V_{xz} = 4690 \pm 10\,,$$

$$V_{yy} = 7145 \pm 2\,, \quad V_{yz} = 4490 \pm 10\,, \quad V_{zz} = 6718 \pm 2\,.$$

Here x, y, and z are the directions along the orthorhombic axes a, b, and c. The corresponding elastic constants are (in units of 10^{11} dyn/cm^2,

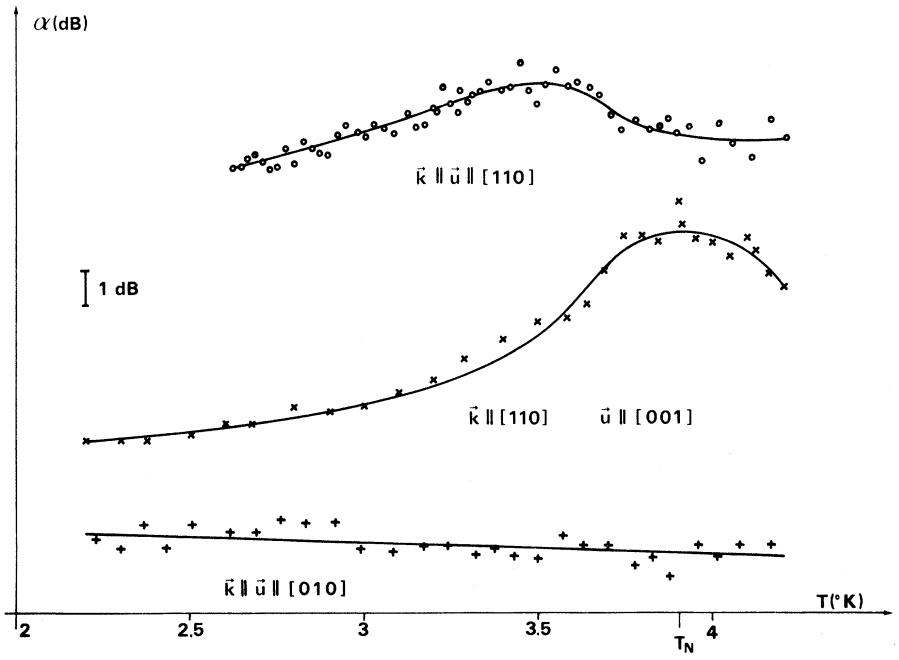

FIG. 8. Ultrasonic attenuation in $GdAlO_3$ as a function of temperature for three different ultrasonic polarizations. Zero magnetic field, $f \sim 9$ GHz.

TABLE II. Experimentally determined magnetoelastic coupling constants.

Ultrasonic wave	$\vec{k} \parallel [110]$ $\vec{u} \parallel [001]$	$\vec{k} \parallel [010]$ $\vec{u} \parallel [010]$	$\vec{k} \parallel [001]$ $\vec{u} \parallel [001]$	$\vec{k} \parallel [110]$ $\vec{u} \parallel [110]$	$\vec{k} \parallel [001]$ $\vec{u} \parallel [010]$
Line observed	Two-magnon line	Two-magnon line	Two-magnon line	AFMR	AFMR
Magnetoelastic constant (cm^{-1})	$\lvert G_{44} \rvert \simeq 0.5$	$\lvert \frac{3}{2}G_{11} - 2G_{44} \rvert \simeq 1.25$	$\lvert G_{11} \rvert \simeq 0.75$	$\lvert G_{11} \rvert \simeq 0.7$	$\lvert G_{44} \rvert \simeq 0.2$

density = 7.43 g/cm^3):

$$C_{11} = 29.12 \pm 0.02\,, \quad C_{22} = 37.93 \pm 0.02\,,$$

$$C_{33} = 33.53 \pm 0.02\,, \quad C_{44} = 14.98 \pm 0.1\,,$$

$$C_{55} = 16.34 \pm 0.1\,, \quad C_{66} = 10.12 \pm 0.1\,.$$

IV. DISCUSSION

Here we shall interpret the experimental result in terms of the theory advanced in Sec. II.

The 9-kG line is attributed to the resonance with the low-frequency spin wave, whereas the 1650-G line arises from a transition between the two spin-wave modes. Two magnetoelastic coupling constants were determined by means of a comparison of the experimental attenuation amplitude and linewidth with the corresponding theoretical expressions. The details are shown in Table II. Two different evaluations based on the two lines observed give compatible results, namely,

$$\lvert G_{11} \rvert = 0.7 \pm 0.2 \text{ cm}^{-1}\,, \quad \lvert G_{44} \rvert = 0.3 \pm 0.2 \text{ cm}^{-1}\,.$$

Furthermore, the selection rules were verified for the antiferromagnetic-acoustic-resonance line. The two-magnon line should also obey selection rules, but its low intensity precludes verification. The maximum absorption of the AFMR line occurs at a magnetic field which varies with temperature. The field variation is shown to be compatible with a mean-field model description.

Study of the position of the AFMR line with respect to the critical field at different temperatures reveals the presence of the soft mode in the AF mode driving the spin-flop transition. This observation of the soft-mode frequency as a function of T_c and H is consistent with the static parameters describing antiferromagnetic $GdAlO_3$, and with electromagnetic AFMR data by Thomas and Rohrer. Observation of the AFMR linewidth gives additional information on the lifetime of spin waves.

The temperature-dependent linewidth can be extrapolated to $T = 0$, where $\Delta H \neq 0$ supposedly arises from inhomogeneities of the crystal. The experimental linewidth can thus be separated in $\Delta H_{\text{expt}} = \Delta H(0) + \Delta H(T)$, where $\Delta H(T) = \{T_2\}$ is attributed to lifetime broadening.

The two-magnon line can also be considered as lifetime broadened, in which case the linewidth should increase with temperature. An alternative possibility is broadening due to transitions between different points of the dispersion curves. An estimate of the "dispersion linewidth" gives a temperature-independent 30 G. Obviously, the experimental results shown in Fig. 5 strongly favor lifetime broadening of the two-magnon line.

At zero magnetic field the attenuation of longitudinal waves along [110] as a function of temperature shows a maximum at 3.5 °K and an effective width of 0.3 °K. The hypothesis that this attenuation is due to resonance with the zero-field magnon is compatible with the magnon position, its lifetime, and the selection rule of the coupling which allows coupling only for wave propagation in the [110] direction. Indeed no attenuation was found for $\vec{k} \parallel \vec{u} \parallel b, c$.

The attenuation maximum for transverse waves right at T_N is supposed to arise from a mechanism connected to the transition. We do not offer any explanation for this attenuation maximum nor for the strong attenuation found for all polarizations in the flop phase, i.e., above 12 kG. A systematic study of this latter problem is under way and will be published later.

V. CONCLUSION

We have demonstrated experimentally the presence of several ultrasonic-absorption mechanisms in $GdAlO_3$. These observations were possible owing to application of high-frequency ultrasound.

Interpretation of the data is supported by a theory of ultrasonic attenuation which takes into account spin-phonon interaction and single-ion magnetostriction. From AFMR data and theory we determine the two magnetoelastic coupling constants G_{11} and G_{44}. This determination of G from AFMR is consistent with the one from the two-magnon resonance, which indicates that the molecular-field approach is adequate in the AF phase of $GdAlO_3$. A comparison of the values for G with those in MnF_2 shows a low coupling constant for $GdAlO_3$ indicating weak coupling of Gd^{3+} spins to the lattice. In particular, the attenuation of sound around the Néel temperature at zero field proved to be too weak to allow con-

clusions to be drawn on the transition mechanism.

ACKNOWLEDGMENTS

We should like to thank Professor J. Joffrin, Dr. A. Levelut, and Dr. H. Rohrer for help with computations and for their continuous interest in this research; also H. J. Scheel for providing $GdAlO_3$ single crystals. We are also grateful to Dr. R. Melcher for commenting on this manuscript at an early stage.

*Associated with the Centre National de la Recherche Scientifique.

[1]K. W. Blazey and H. Rohrer, Helv. Phys. Acta 40, 370 (1967).

[2]K. W. Blazey and H. Rohrer, Phys. Rev. 173, 574 (1968).

[3]J. D. Cashion, A. H. Cooke, T. L. Thorp, and M. R. Wells, Proc. Roy. Soc. (London) A318, 473 (1970).

[4]J. F. B. Hawkes and M. J. M. Leask, J. Phys. C 1, 165 (1968).

[5]K. W. Blazey, K. A. Müller, M. Ondris, and H. Rohrer, Phys. Rev. Letters 24, 105 (1970).

[6]M. Boiteux, P. Doussineau, B. Ferry, and U. T. Höchli, J. Phys. (Paris) Suppl. 32, 496 (1971).

[7]K. W. Blazey, H. Rohrer, and R. Webster, Phys. Rev. B 4, 2287 (1971).

[8]H. Rohrer and H. Thomas, J. Appl. Phys. 40, 1025 (1969).

[9]S. Geller and B. Bala, Acta Cryst. 9, 1019 (1956).

[10]P. Doussineau, thesis (Université Paris VI, 1971) (unpublished).

[11]A. Herpin and P. Mériel, Compt. Rend. 259, 2415 (1964).

[12]Y. Shapira and J. Zak, Phys. Rev. 170, 503 (1968).

[13]F. Keffer, in *Handbuch der Physik*, edited by S. Flügge (Springer-Verlag, Berlin, 1966), Vol. XVIII/2.

[14]R. K. Wangness, Phys. Rev. 98, 927 (1955).

[15]H. Thomas, in *Proceedings of the Chania International Conference on Magnetism*, 1969 (Gordon and Breach, New York, to be published), Vol. 8.

[16]H. Thomas and H. Rohrer (unpublished).

[17]F. Keffer and C. Kittel, Phys. Rev. 85, 329 (1952).

[18]I. Waller, Z. Physik 79, 370 (1932).

[19]B. Lüthi, T. J. Moran, and R. J. Pollina, J. Phys. Chem. Solids 31, 1741 (1970).

[20]S. A. Al'tshuler, B. I. Kochelaev, and A. M. Leushin, Usp. Fiz. Nauk SSSR 75, 459 (1961) [Sov. Phys. Usp. 4, 880 (1962)].

[21]D. H. MacMahon and R. H. Silsbee, Phys. Rev. 135, A91 (1964).

[22]J. H. Van Vleck, Phys. Rev. 57, 426 (1940).

[23]D. E. Eastman, Phys. Rev. 148, 539 (1966).

[24]R. L. Melcher, Phys. Rev. Letters 25, 1201 (1970).

[25]$\Delta M = 2$ process is theoretically possible via the volume magnetostriction, as it has been shown by R. Silberglitt [Phys. Rev. 188, 786 (1969)] in the case of ferromagnets. However, such a process involves phonons with energy greater than that of $k = 0$ spin waves; this is not the case considered here.

[26]E. H. Jacobsen, Phys. Rev. Letters 2, 249 (1959).

[27]H. J. Scheel and E. O. Schulz-Dubois, J. Cryst. Growth 8, 304 (1971); H. J. Scheel, *ibid.* 13/14, 1 (1972).

PHYSICAL REVIEW B VOLUME 6, NUMBER 7 1 OCTOBER 1972

Magnetic Anisotropy of Tetrahedral Ferrous Ions in $CdCr_2S_4$

B. Hoekstra, R. P. van Stapele, and A. B. Voermans
Philips Research Laboratories, Eindhoven, Netherlands
(Received 20 March 1972)

The magnetic anisotropy of single crystals of the ferromagnetic cubic spinel $Cd_{1-x}Fe_xCr_2S_4$ with $x = 0.005$, 0.01, and 0.02 was studied by ferromagnetic resonance at 9 and 34 GHz. The anisotropy observed at 4.2 K can be explained on the basis of strongly anisotropic Fe^{2+} ions on cubic tetrahedral sites. In the crystal field model used, the cubic ^5E ground state is split by exchange and spin-orbit interactions. The model provides a good description of the temperature-dependent anisotropy at temperatures below 15 K, with $\Delta_{ex} \gtrsim 200$ cm^{-1} and $\delta = 6(\lambda^2/\Delta_c + \rho) = 13 \pm 1$ cm^{-1}.

I. INTRODUCTION

The cubic spinel crystal $FeCr_2S_4$ is known to exhibit a large magnetocrystalline anisotropy at temperatures below 50 K. This anisotropy has been attributed to the single-ion anisotropy of the ferrous ion on the tetrahedral site.[1] From magnetization data it was shown that the cubic axis is the preferred direction. Mössbauer experiments by Eibschütz *et al.*[2] showed the presence of a quadrupole splitting which has the same origin as the anisotropy. However, Hoy and Singh[3] observed a deviation from axial symmetry in the Mössbauer spectrum between 61 and 186 K. The spectrum at 4.2 K shows very clearly the presence of low-symmetry crystalline fields.[1]